Uncertainty in Aerosol Radiative Forcing Impacts the Simulated Global Monsoon in the 20th Century

Jonathan K. P. Shonk[1, *], Andrew G. Turner[1, 2], Amulya Chevuturi[1], Laura J. Wilcox[1], Andrea J. Dittus[1] and Ed Hawkins[1]

[1] National Centre for Atmospheric Science, University of Reading, Reading, UK
[2] Department of Meteorology, University of Reading, Reading, UK
[*] Current affiliation: Met Office @ Reading, University of Reading, Reading, UK

Corresponding author: Jonathan K. P. Shonk (current e-mail address: jon.shonk@metoffice.gov.uk)

Abstract. Anthropogenic aerosols are dominant drivers of historical monsoon rainfall change. However, large uncertainties in the radiative forcing associated with anthropogenic aerosol emissions, and the dynamical response to this forcing, lead to uncertainty in the simulated monsoon response. We use historical simulations in which aerosol emissions are scaled by factors from 0.2 to 1.5 to explore the monsoon sensitivity to aerosol forcing uncertainty (-0.38 W m^{-2} to -1.50 W m^{-2}). Hemispheric asymmetry in emissions generates a strong relationship between scaling factor and both hemispheric temperature contrast and meridional location of tropical rainfall. Increasing the scaling from 0.2 to 1.5 reduces the global monsoon area by 3% and the global monsoon intensity by 2% over the period 1950–2014, and switches the dominant influence on the 1950–1980 monsoon rainfall trend between greenhouse gas and aerosol. Regionally, aerosol scaling has a pronounced effect on Northern Hemisphere monsoon rainfall.

1 Background

Monsoon systems provide rainfall for billions of people, many of whom are dependent on the monsoon rains for survival. It is therefore important to understand the effects of climate change on the global monsoon, both in the past and future. Projections show a future increase in global monsoon area, rainfall amount, and rainfall intensity (Hsu et al., 2012, 2013). In contrast, studies have reported a decline in global monsoon rainfall in the latter half of the 20th century (Hsu et al., 2011; Wang & Ding, 2006; Zhou et al., 2008), particularly in Northern Hemisphere (NH) monsoons (Zhou et al., 2008).

Historical emissions of anthropogenic aerosols (AA) and their precursors cause negative radiative forcing, global cooling and suppression of rainfall, hence opposing the impacts of greenhouse gas (GHG) emissions (Wu et al., 2013). Furthermore, most AA emissions arise in the NH, giving them a strong control on hemispheric temperature gradients (e.g., Wilcox et al., 2013), with profound effects on monsoon circulations (Broccoli et al., 2006; Friedman et al., 2013; Voigt et al., 2017) and interhemispheric energy and moisture transport (Haywood et al., 2016; Stephens et al., 2016). Recently, large-scale AA-driven circulation changes have acted to weaken the monsoon, and have dominated over the response to GHG. Bollasina et al. (2011), Polson et al. (2014), Salzmann et al. (2014), Song et al. (2014) and Guo et al. (2015) have all shown that increasing AA

emissions played an important part in driving regional and global monsoon rainfall decrease during the mid-20th century. However, in future, a GHG-driven thermodynamic response is expected to dominate, driving increased monsoon rainfall (Li et al., 2015).

Land-sea contrasts affect temperature gradients and thus also affect monsoon circulation strength. On regional scales, AA-induced cooling can oppose GHG-induced warming effects (Ramanathan et al., 2005; Ramanathan & Feng, 2009), leading to a slackening of temperature contrasts between land and sea (Lau & Kim, 2017) and an increase in surface pressure (Song et al., 2014), both of which weaken the circulation. Remote AA emissions are also important, acting to change monsoon rainfall through circulation changes, albeit via different mechanisms to local AA emissions (Cowan & Cai, 2011; Dong et al., 2016; Undorf et al., 2018; Wang et al., 2017). Within regional monsoon systems, AA emissions can also change the characteristics and distribution of rainfall, affecting monsoon onset (Lau et al., 2006) and withdrawal (Guo et al., 2016).

In future climate projections, in which AA emissions look likely to decrease while GHG emissions continue to increase, the ability to capture the balance between their respective radiative effects is crucial. Future reductions in AA emissions have the potential to cause increases in global rainfall comparable to those resulting from moderate GHG increases (Rotstayn et al., 2013), with the largest increases anticipated over East and South Asia (Levy et al., 2013; Westervelt et al., 2015). However, there is substantial uncertainty in present-day top-of-atmosphere aerosol effective radiative forcing, with a 5%-to-95% confidence interval spanning -1.9 W m^{-2} to -0.1 W m^{-2} (Myhre et al., 2013). Uncertainty in the magnitude of aerosol forcing, and the monsoon response to it, is compounded in climate projections, where potential aerosol emission pathways are diverse. In the Asian region in particular, there is great variety in future emission trends across the Shared Socio-Economic Pathways (SSPs). Of particular importance for the monsoon is the uncertainty in the sign of the projected emission trends over China and India depending on the SSP (Samset et al., 2019; Figure 1b).

In this study, we quantify the impact of the uncertainty in present-day aerosol radiative forcing on the global monsoon system using a set of historical climate simulations produced as part of the SMURPHS ("Securing Multidisciplinary Understanding and Prediction of Hiatus and Surge Events") project (Dittus et al., 2020). The SMURPHS ensemble consists of a set of historical climate simulations with AA emissions scaled by various factors, allowing us for the first time to investigate the sensitivity of the climate system to the strength of the forcing. Such an investigation is challenging in a multi-model framework (such as the AA-only simulations of CMIP5; Taylor et al., 2012) since differences in model biases and parameterisations introduces additional uncertainties in the response to forcing, preventing an assessment of the influence of forcing uncertainty alone. We introduce the ensemble and experimental design in more detail in Section 2. The effect of the aerosol scaling in terms of temperature contrasts across hemispheres, and between land and sea, is examined in Section 3. Section 4 presents the effects of scaling on standard metrics of the global and regional monsoons. We summarise and conclude in Section 5.
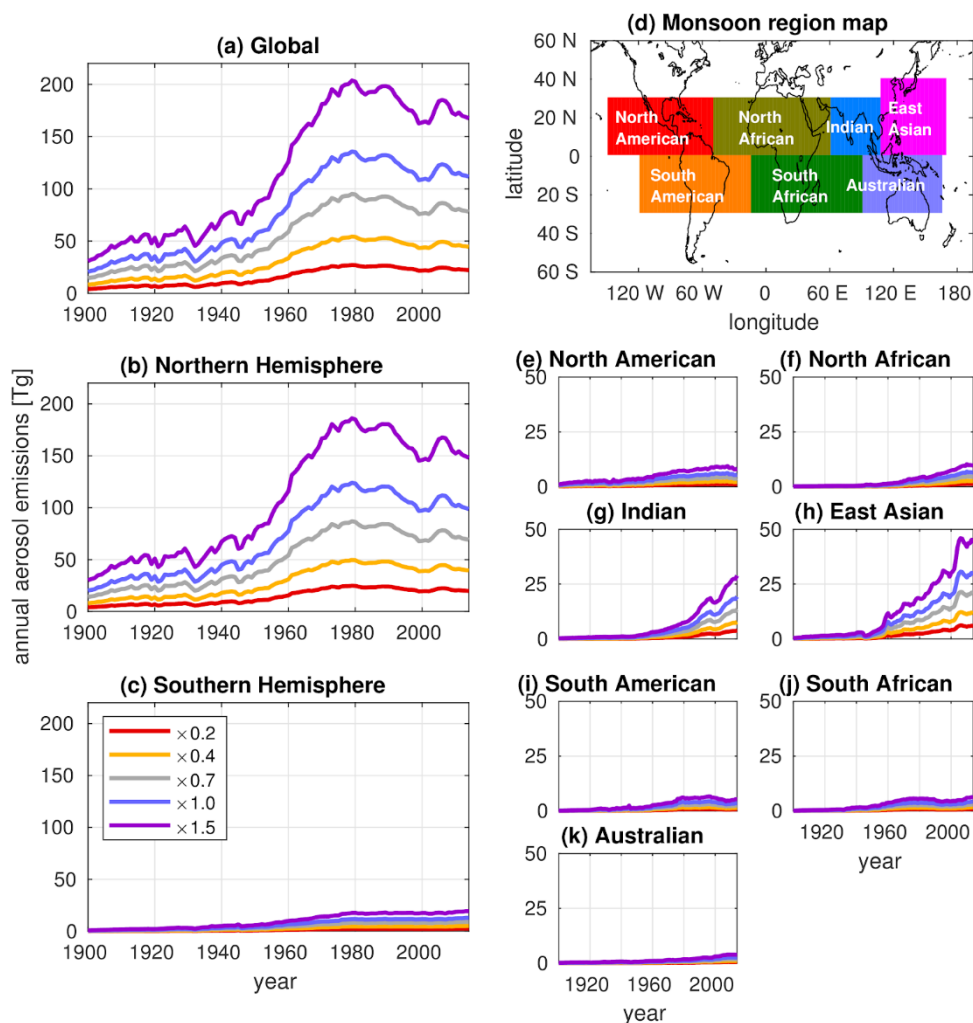
Figure 1. Sulphur dioxide emissions used in SMURPHS on (a) global, (b, c) hemispheric and (e–k) regional scales, in Tg yr^{-1}. Organic and black carbon emissions are scaled in the same way. Monsoon regions are as defined in panel (d).

2 SMURPHS ensemble and aerosol emission data

The SMURPHS dataset consists of historical climate simulations run over the period 1850–2014 using a fully coupled version of HadGEM3-GC3.1 at resolutions of N96 and 1° in the atmosphere and ocean respectively (Kuhlbrodt et al., 2018; Williams et al., 2018). The model version used here is a development version towards the UK submission to CMIP6 (Andrews et al, 2020; Dittus et al., 2020; Hardiman et al., 2019). HadGEM3 uses the GLOMAP two-moment aerosol scheme that includes representations of the cloud albedo and cloud lifetime effects (Mulcahy et al., 2018 and references therein). Five ensemble members are run for each of five experiments in which the historical aerosol emissions are scaled by a constant factor. This factor is applied to emissions of all species of anthropogenic aerosol and precursors, at all locations throughout the historical

emissions dataset. Five scaling factors were selected: ×0.2, ×0.4, ×0.7, ×1.0 and ×1.5, with the ×1.0 scaling corresponding to the standard CMIP6 historical protocol. The scaling factors were chosen to sample a broad range of the uncertainty in present-day aerosol radiative forcing according to Myhre et al. (2013), and correspond to forcings of −0.38 W m^{-2}, −0.60 W m^{-2}, −0.93 W m^{-2}, −1.17 W m^{-2} and −1.50 W m^{-2} respectively. More detail on the SMURPHS ensemble is presented by Dittus et al.
5 (2020). The performance of HadGEM3 in representing various monsoon properties is compared against observations and reanalysis in the Appendix (Figure A1), in which we demonstrate the fidelity with which the model reproduces the monsoon properties evaluated in this study.

The SMURPHS simulations use the same aerosol emission dataset as used in CMIP6 (Hoesly et al., 2018), which contains emissions from 1750–2014 for sulphur dioxide, black carbon and organic carbon. Sulphur dioxide emissions from 1900
10 onwards are shown in Figure 1. In the early 20th century, emissions increased gradually, but then ramped up from 1950 to 1980. Since 1980, emission mitigation efforts in North America and Europe have been balanced by continued increases in Asia, causing global emissions to level off. The hemispheric asymmetry in AA emissions is clear, with the NH contributing approximately 90% of the global total throughout the 20th century (Figures 1b, 1c). Most monsoon regions show a gradual increase in emissions in the 20th century, with pronounced increases since 1970 seen in the Indian and East Asian sectors
15 (Figures 1g, 1h). The Hoesly et al. (2018) emissions dataset is the most up-to-date inventory of historical AA emissions and is therefore considered the best estimate.

In this study, we use all five members from each of the five experiments, but include years from 1900 onwards, to allow 50 years for the model to adjust to the scalings (after Dittus et al., 2020). When considering climatological quantities, we consider the ensemble mean for each experiment to be the model estimate of the climate system under those scaling conditions and
20 indicate uncertainty across ensemble members in terms of inter-member standard deviation. Where quantities are averaged over areas, a cosine-based latitude weighting is applied.

3 Temperatures and contrasts

The effect of AA on global mean temperature is clear (Figure 2a). Higher aerosol scalings lead to cooler global temperatures, and by the 1970–2014 period there is little overlap in global temperature between scalings. We also see evidence of the control
25 by AA emissions on the mid-20th-century hiatus (the period 1950–1980), in agreement with the findings of Wilcox et al. (2013) and Jones et al. (2013). The higher scalings lead to a stronger hiatus; the lower scalings lead to a much weaker hiatus. In the ×0.2 experiment, a hiatus is barely discernible. These results echo those of Dittus et al. (2020).

The hemispheric asymmetry of AA emissions leads to a much greater degree of cooling in the NH, so the strength of the forcing has a control on the hemispheric temperature contrast (HTC), defined as NH minus SH (Chang et al., 2011; Wilcox et
30 al., 2013). Lower scalings reduce the degree of NH cooling and therefore increase the HTC (Figure 2b). The NH is, on average, warmer than the Southern Hemisphere (SH; for example, Kang et al., 2015) although, under the highest scaling (×1.5), the HTC reverses in sign during the 1970s and 1980s.
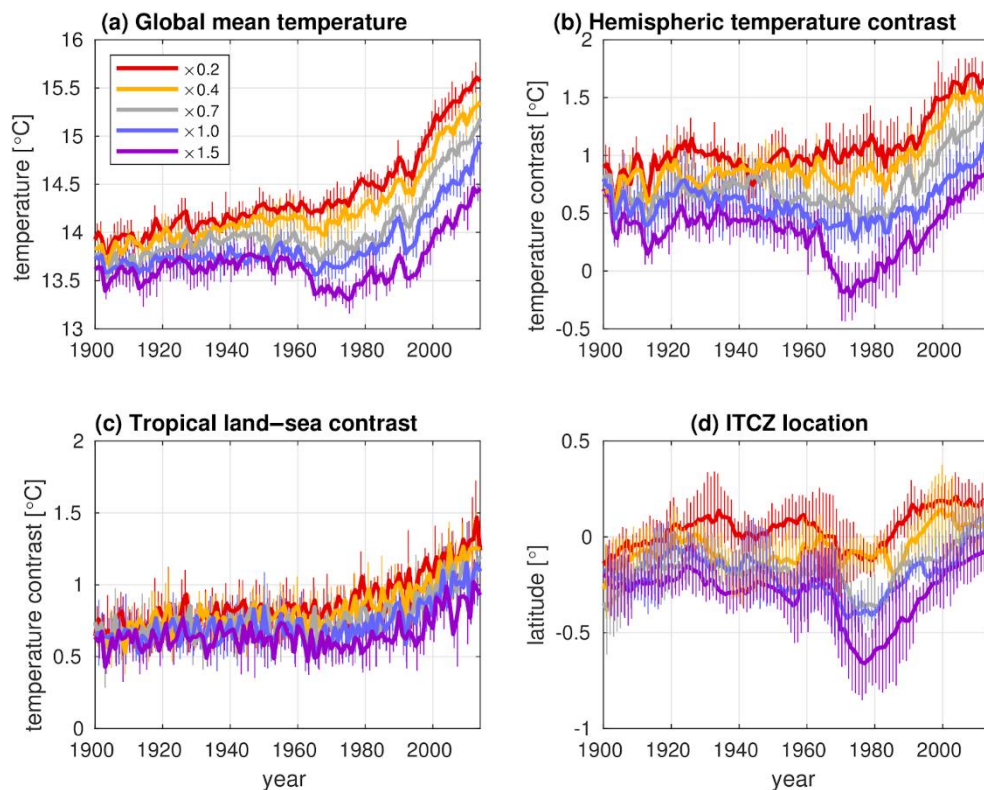
Figure 2. Time series of various atmospheric properties from the SMURPHS simulations: (a) global mean surface air temperature; (b) hemispheric temperature contrast (NH minus SH); (c) tropical land–sea temperature contrast, calculated in the summer months (November–March in SH, May–September in NH) for latitudes within 30° S and 30° N only; (d) global mean ITCZ location, calculated following Shonk et al. (2018). All values are ensemble means; vertical error bars indicate one standard deviation across the five ensemble members.

This shift in HTC is reflected in the location of the ITCZ. We calculate ITCZ location using the method of Shonk et al. (2018), the ITCZ at a given longitude being defined as the latitude centroid of the region of rainfall that exceeds 50% of the maximum value at that longitude. The ITCZ location presented here (Figure 2d) is the zonal mean value (note that the general location of the ITCZ south of the equator is caused by the inclusion of the Southern Pacific and Atlantic Convergence Zones). Lower scalings, associated with a warmer NH and stronger HTC, lead to an ITCZ location that is further north, consistent with Hwang et al. (2013), Allen et al. (2015) and Chung and Soden (2017).

Monsoon strength is also influenced by changes in the land–sea temperature contrast (LSTC), both on regional (Lau & Kim, 2017) and global (Fasullo, 2012) scales. While weaker than the effect on HTC, there is a degree of control of the aerosol scaling on the LSTC, albeit with a larger overlap between ensemble members (Figure 2c). Higher scalings result in cooler land surfaces with respect to the surrounding oceans, hence the LSTC is reduced, and the monsoon is weakened.

The control of the aerosol forcing on the properties presented in this section is demonstrated quantitatively in the top section of Table 1 in terms of means over the 1950–2014 period, when most changes in anthropogenic aerosol have occurred. All properties vary monotonically and roughly linearly across the range of scalings used in SMURPHS, with higher scalings

resulting in a cooler global temperature, a weaker HTC, an ITCZ situated further south, and a weaker LSTC. The impact of the uncertainty in present-day forcing on these properties is presented in the rightmost column of Table 1 as the differences between the lowest and highest scalings (×1.5 minus ×0.2). Changing the forcing from lowest to highest value lowers global temperature by nearly 1 °C and reduces the HTC from 1.19 °C to 0.27 °C. The zonal-mean ITCZ location shifts southwards

5 by 0.41° of latitude, and the LSTC reduces by just over 30%, from 0.98 °C to 0.68 °C.

Table 1. Mean monsoon-related properties, as defined in Sections 3 and 4, averaged over the period 1950–2014 (during which global aerosol emissions increased), and all five ensemble members. The difference column is the change from ×0.2 (lowest scaling) to ×1.5 (highest scaling), expressed as a percentage where indicated.

	×0.2	×0.4	×0.7	×1.0	×1.5	Difference
Global mean temperature [°C]	14.67	14.48	14.21	13.99	13.71	**−0.95**
Hemispheric temperature contrast [°C]	1.19	1.03	0.78	0.57	0.27	**−0.91**
ITCZ location (latitude) [°]	0.05	−0.03	−0.15	−0.24	−0.36	**−0.41**
Tropical land–sea contrast [°C]	0.98	0.92	0.83	0.77	0.68	**−0.30**
GMA [Mm^2]	126.8	126.0	125.0	124.3	122.8	**−2.99%**
HMA (NH) [Mm^2]	66.8	66.0	65.5	64.9	63.9	**−4.25%**
HMA (SH) [Mm^2]	60.0	59.9	59.5	59.5	59.0	**−1.60%**
GMI [mm d^{-1}]	7.76	7.74	7.69	7.66	7.61	**−1.93%**
HMI (NH) [mm d^{-1}]	7.68	7.65	7.57	7.54	7.48	**−2.58%**
HMI (SH) [mm d^{-1}]	7.86	7.84	7.82	7.78	7.76	**−1.30%**

10 ## 4 Monsoon area and rainfall

We evaluate the effects of aerosol scaling on the monsoon via Global Monsoon Area (GMA) and Global Monsoon Intensity (GMI). These properties are defined following Liu et al. (2009), Hsu et al. (2011) and others: a gridbox is within the GMA if the difference in summer and winter rainfall (May to September and November to March, depending on hemisphere) is greater than 2 mm d^{-1}, and more than 55% of the rain falls in the summer months. The total GMA is calculated as the sum of the area

15 of all gridboxes within the GMA region. GMI is then calculated as the total rainfall within the GMA, divided by the area of the GMA. We also define hemispheric equivalents (HMA and HMI) – these are the GMA and GMI calculated separately for each hemisphere.
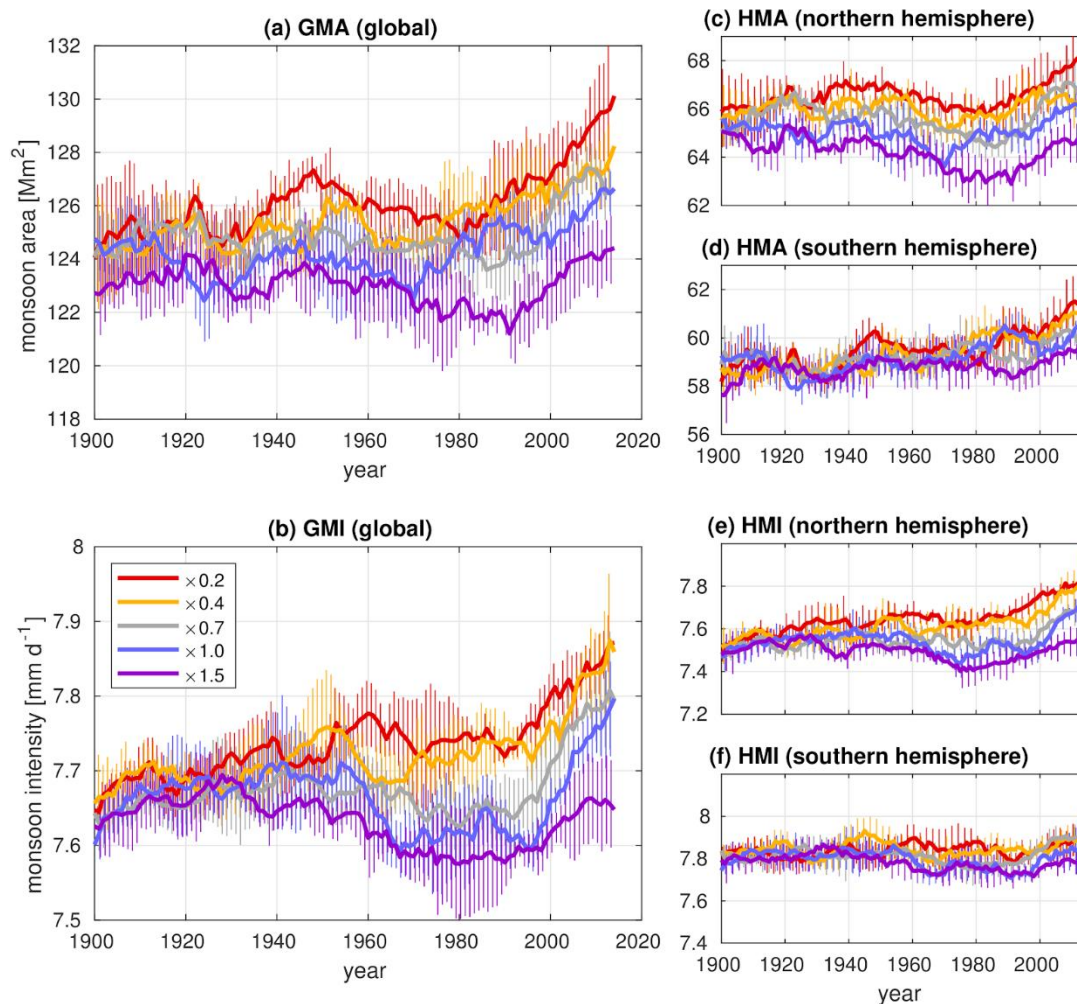
Figure 3. Time series of (a) global monsoon area (GMA) and (b) global monsoon intensity (GMI) for each experiment. Panels (c, d) and (e, f) show the hemispheric equivalents (HMA and HMI) for NH and SH. The ensemble mean is shown, with an 11-year running mean applied. The vertical error bars indicate the standard deviation across the four members. GMA is in Mm², where 1 Mm² = 1 × 10⁶ km².

Both GMA and GMI show a dependence on AA forcing (Figures 3a, 3b), with a higher scaling leading to a reduction of both intensity and area. This is consistent with the effects of the scaling on global temperature, HTC and LSTC, which are also reduced at higher scalings. This dependence is clearest in GMI from 1950–1980: during this period, higher scalings produce a greater weakening of the GMI than lower scalings. This suggests a switch between GHGs and AAs dominating the influence on the monsoon from 1950–1980 across the range of uncertainty in aerosol forcing. The dependence is also clear in GMA, although the timing, duration, and strength of the GMA reduction after 1950 vary across scalings. This is most likely associated with natural variability across the five ensemble members.

Despite this variability, the effect of the scalings on GMA and GMI when averaged over 1950–2014 is also monotonic and roughly linear with scaling factor across the experiments (Table 1). The effect of the uncertainty in aerosol radiative forcing

on GMA and GMI is a reduction of 2.99% and 1.93% respectively, when increasing the scaling across its range. For context, Hsu et al. (2013) found that 1 °C of warming in CMIP5 models resulted in multi-model mean increases of 1.9% and 1.3% in GMA and GMI (see their Figure 5). The sensitivities identified here are higher (about 3.1% and 2.0% per °C), although lie well within the range of sensitivities presented by Hsu et al. (2013).
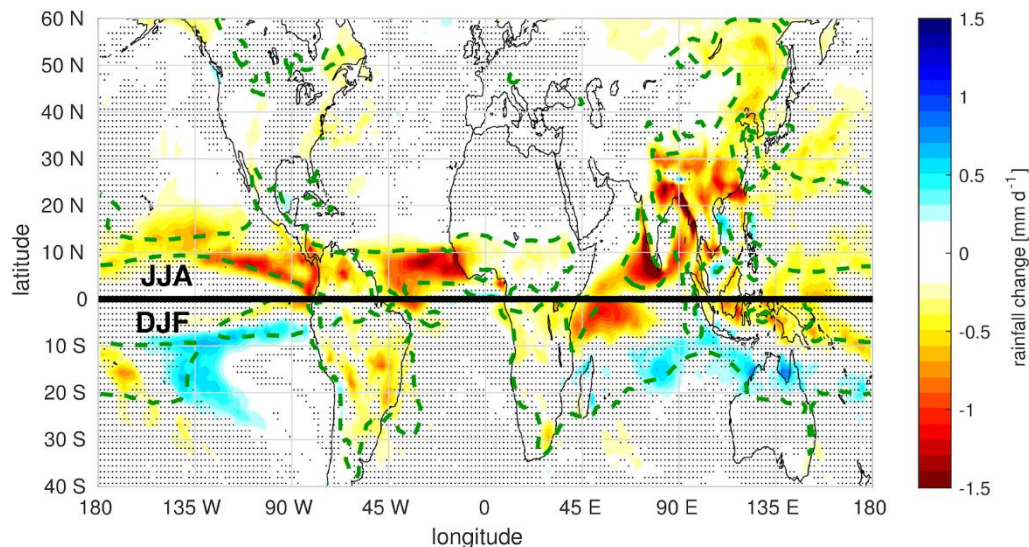
Figure 4. The difference in monsoon rainfall (in mm d⁻¹) across the range of the scaling factors (×1.5 minus ×0.2). The summer months are shown in each hemisphere (June–August in the NH, December–February in the SH); the thick black line marks the equator. Averaged over the period 1950–2014, and across all ensemble members. The green dotted line indicates the mean GMA in the ×1.0 experiment. Spots indicate regions where the rainfall difference is insignificant with respect to variability across years and
10 **members.**

The effects of aerosol scaling on both GMA and GMI are dominated by the NH, with a weak dependence on the scaling found in the SH (Figures 3c–3f). The effect of uncertainty in aerosol radiative forcing has substantial effects on the rainfall in the regional monsoons (Figure 4), with the greatest rainfall changes in the NH monsoons. The North American and North African monsoon experience a marked reduction, while the decrease in the Asian monsoon is even greater (consistent with the much
15 larger aerosol emissions originating there; see Figures 1g, 1h). The effect of the scaling on the SH monsoons, in contrast, is much more variable, reflecting the much smaller aerosol forcing there. The effect of the aerosol forcing uncertainty on HMA and HMI from 1950 onwards in the NH is more than twice that in the SH (Table 1).

On account of the complexity of monsoon behaviours in different regions (see Section 1), we defer a full quantitative analysis of the regional monsoons to a future study. To encourage and motivate this work, we include regional versions of Figure 3 and
20 Table 1 in the Appendix. Furthermore, we further encourage modelling centres to perform their own SMURPHS-style ensembles to allow inter-model comparison of the impacts of aerosol uncertainty.

5 Summary and conclusions

The observed reduction in global monsoon area and intensity since 1950 has been widely attributed to a rapid increase in emissions of anthropogenic aerosols and their precursors. The cooling associated with these emissions is concentrated in the Northern Hemisphere, and opposes the warming effect of greenhouse gases and reduces the temperature contrast between
5   hemispheres and between land and sea. This has been shown to weaken the monsoon circulations, resulting in a reduction of monsoon rainfall. Understanding the interplay between aerosol forcing and monsoon properties in past simulations is important in order to constrain future monsoon projections, where anthropogenic aerosol reductions are likely to strengthen the monsoon, in addition to the strengthening anticipated in response to further increases in greenhouse gases.

We explored the sensitivity of the global monsoon to uncertainty in historical aerosol radiative forcing using an ensemble of
10   simulations in which anthropogenic aerosol and precursor emissions from 1850–2014 are scaled by factors ranging from ×0.2 to ×1.5 (corresponding to a present-day aerosol effective radiative forcing range of −0.38 W m^{-2} to −1.50 W m^{-2}). When averaged over the period 1950–2014, increasing the scaling factor across this range results in a 0.95 °C cooling of global temperature, a 75% reduction in hemispheric temperature contrast, a 30% reduction in land–sea temperature contrast, and a southward shift of the ITCZ by 0.4° of latitude. The global monsoon area is reduced by 3% and the intensity of the rainfall
15   within this region is reduced by 2%. Regionally, much of the reduction in monsoon area and intensity arises in the Northern Hemisphere monsoons, particularly the Asian sector, where emission changes are greatest.

Long-term monsoon variability since 1950 has very different characteristics across the scaling factors. In the ×1.5 experiment, an overall negative trend in monsoon rainfall intensity is found, dominated by strong aerosol forcing; in the ×0.2 experiment, greenhouse gases are able to dominate and monsoon intensity increases. Reducing uncertainty in the radiative forcing
20   associated with anthropogenic aerosol would provide more reliable estimates of the future evolution of global and regional monsoons as anthropogenic aerosol and precursor emissions decline.

Appendix: validation and regional figures

This Appendix validates the performance of the model used in the SMURPHS simulations against various observation datasets (Figure A1). It then demonstrates the effect of the scaling on the individual monsoon regions, in terms of regional monsoon
25   area (RMA; Figure A2) and regional monsoon intensity (RMI; Figure A3), presented in the style of Figure 3. It concludes with a table of RMA and RMI values for the monsoon regions, averaged over the years 1950 to 2014 in the style of Table 1.
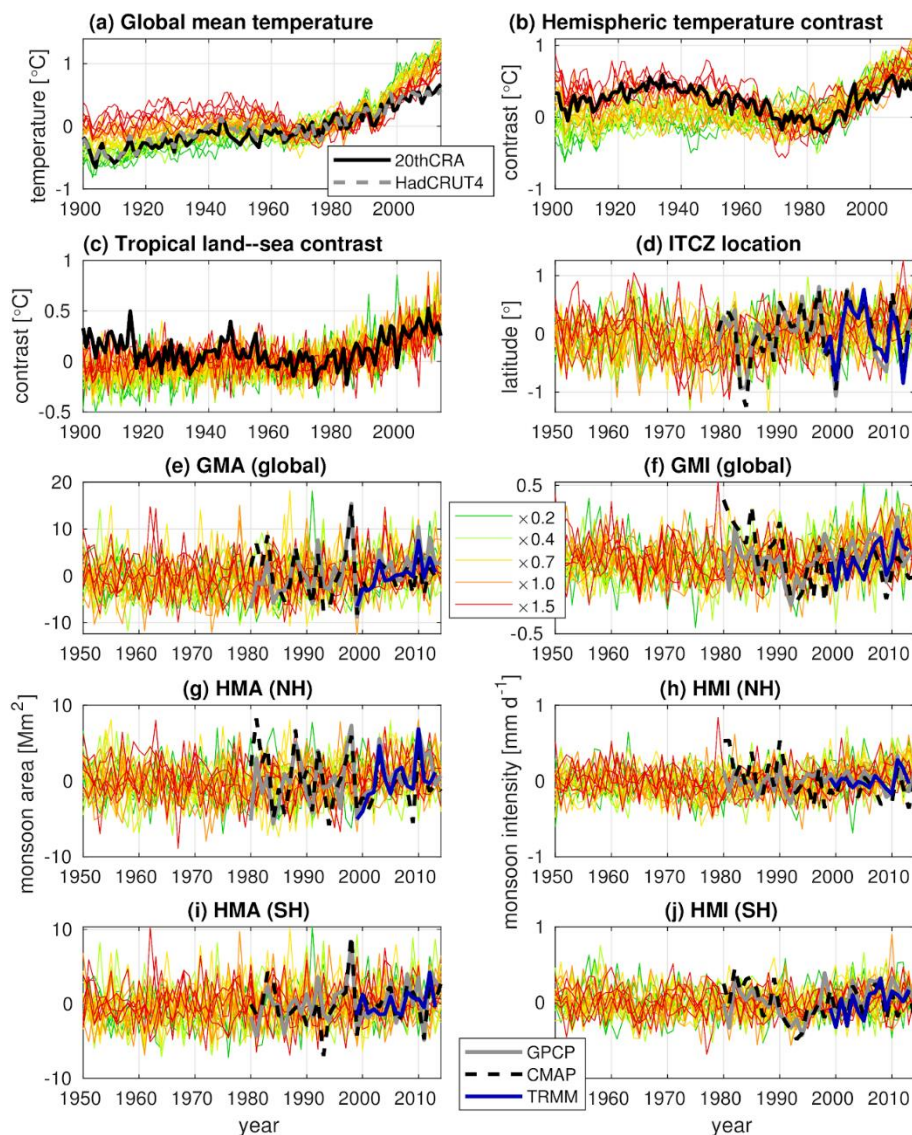
Figure A1. Validation time series comparing the model used in the SMURPHS ensembles (HadGEM3) with observation and reanalysis datasets. For temperature quantities, we use data from 20th Century Reanalysis (20thCRA; Slivinski et al., 2019) and Hadley Centre/Climatic Research Unit Temperature (HadCRUT4; Morice et al., 2012). For rainfall quantities, we use data from the
5 **Global Precipitation Climatology Project (GPCP; Adler et al., 2003), the CPC Merged Analysis of Precipitation (CMAP; Xie & Arkin, 1997) and the Tropical Rainfall Measuring Mission (TRMM; Kummerow et al., 2000). All model ensemble members are shown, with no running means as used in Figure 3. Temperature properties span the period 1900 to 2014; rainfall properties span 1950 to 2014. The main paper text describes how the variables are calculated. Anomalies are calculated for each dataset and each experiment, with respect to 1961–1990 (temperature fields) and 1980–2009 (rainfall fields). All variables presented in this paper**
10 **compare well between model and observations in terms of interannual variability and long-term trends. The exception is global temperature since 2000, in which the model produces an accelerated rate of warming, although this is a recognised behaviour (Dittus et al., 2020).**
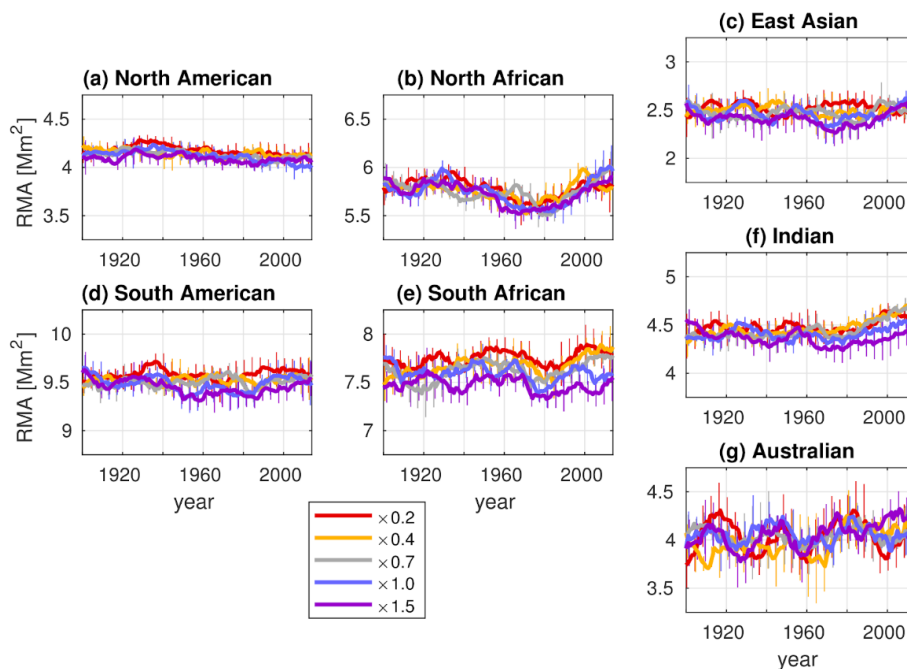
Figure A2. Time series of the regional monsoon area (RMA), following the style of Figure 3. Here, the RMA is defined as the global monsoon area (GMA) that falls over land points within each monsoon region. Regions are as defined in Figure 1d.
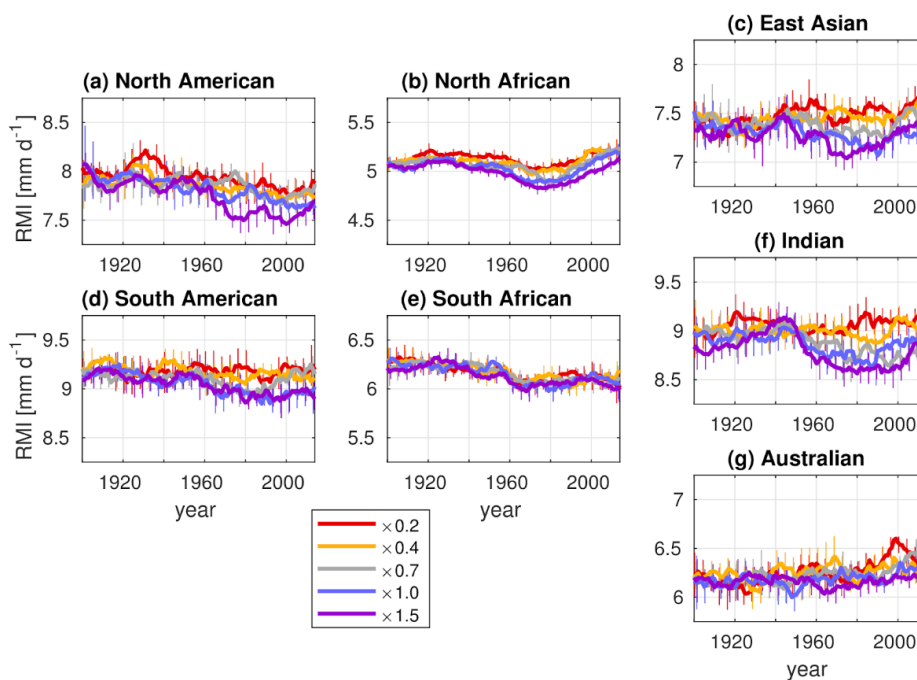
Figure A3. As Figure A2, but for regional monsoon intensity (RMI), defined as the total rainfall within the RMA divided by the area of the RMA.

Table A1. Values of regional monsoon area (RMA), averaged over the years 1950–2014 and all five ensemble members. The difference column is the change from ×0.2 (lowest scaling) to ×1.5 (highest scaling), expressed as a percentage. RMA is defined as in the caption of Figure A2.

	×0.2	×0.4	×0.7	×1.0	×1.5	Difference
RMA (North American) [Mm^2]	4.14	4.13	4.10	4.08	4.08	**−1.78%**
RMA (South American) [Mm^2]	9.58	9.53	9.52	9.46	9.40	**−1.82%**
RMA (North African) [Mm^2]	5.73	5.73	5.73	5.70	5.66	**−1.13%**
RMA (South African) [Mm^2]	7.80	7.70	7.65	7.57	7.46	**−4.16%**
RMA (Indian) [Mm^2]	4.51	4.52	4.49	4.42	4.34	**−3.59%**
RMA (Australian) [Mm^2]	4.04	4.03	4.03	4.05	4.10	**+1.48%**
RMA (East Asian) [Mm^2]	2.52	2.48	2.48	2.46	2.40	**−4.69%**

Table A2. Values of regional monsoon intensity (RMI), laid out as in Table A1. RMI is defined in the caption of Figure A3.

	×0.2	×0.4	×0.7	×1.0	×1.5	Difference
RMI (North American) [mm d^{-1}]	7.87	7.81	7.82	7.74	7.63	**−3.06%**
RMI (South American) [mm d^{-1}	9.19	9.14	9.08	8.98	8.98	**−2.26%**
RMI (North African) [mm d^{-1}]	5.12	5.09	5.05	5.01	4.94	**−3.46%**
RMI (South African) [mm d^{-1}]	6.11	6.11	6.10	6.09	6.06	**−0.83%**
RMI (Indian) [mm d^{-1}]	9.06	9.00	8.80	8.81	8.70	**−4.00%**
RMI (Australian) [mm d^{-1}]	6.33	6.29	6.29	6.21	6.16	**−2.75%**
RMI (East Asian) [mm d^{-1}]	7.53	7.49	7.37	7.25	7.23	**−4.03%**

Data Availability

The data are currently being archived at the UK Centre for Environmental Data Analysis and will be available by the publication date. Meanwhile, a repository containing a subset of the data that is used in this study has been made available for review purposes only here: http://gws-access.ceda.ac.uk/public/smurphs/SMURPHS/.

5 **Author Contribution**

This study used data from the SMURPHS project and provided by AJD and EH. Analysis of the data was performed by JKPS, AGT, AC and LJW. The manuscript was prepared by JKPS with contributions from all co-authors.

Competing Interests

The authors declare that they have no conflict of interest.

10 **Acknowledgements**

This work was funded by the SMURPHS, REAL Projections, and EMERGENCE projects under the Natural Environment Research Council (NERC; Grants NE/N006054/1, NE/N018591/1, and NE/S004890/1 respectively). EH and the SMURPHS ensemble were additionally supported by the National Centre for Atmospheric Science. AC was supported by the Climate Science for Services Partnership (CSSP) China project funded by the Newton Fund. We acknowledge the use of the Monsoon2
15 system, a collaborative facility supplied under the Joint Weather and Climate Research Programme, a strategic partnership between the UK Met Office and NERC.

REFERENCES

Adler, R. F., Huffman, G. J., Chang, A., Ferraro, R., Xie, P., Janowiak, J., et al. The Version-2 Global Precipitation Climatology
20   Project (GPCP) monthly precipitation analysis (1979–present). *Journal of Hydrometeorology* 4, 1147—1167, https://doi.org/10.1175/1525-7541(2003)004<1147:TVGPCP>2.0.CO;2 (2003).

Allen, R. J., Evan, A. T., & Booth, B. B. B. Interhemispheric aerosol radiative forcing and tropical precipitation shifts during the late twentieth century. *Journal of Climate* 28: 8219—8246, https://doi.org/10.1175/jcli-d-15-0148.1 (2015).

Andrews, M. B., Ridley, J. K., Wood, R. A., Andrews, T., Blockley, E. W., Booth, B. B. B., et al. Historical simulations with
25   HadGEM3-GC3.1 for CMIP6. Accepted in *Journal of Advances in Modelling Earth Systems,* https://doi.org/ 10.1029/2019MS001995 (2020).

Bollasina, M. A., Ming, Y., & Ramaswamy, V. Anthropogenic aerosols and the weakening of the South Asian summer monsoon. *Science* 334, 502—505, https://doi.org/10.1126/science.1204994 (2011).

Broccoli, A. J., Dahl, K. A., & Stouffer, R. J. Response of the ITCZ to northern hemisphere cooling. *Geophysical Research Letters* 33, L01702, https://doi.org/10.1029/2005gl024546 (2006).

5 Chang, C. Y., Chiang, J. C. H., Wehner, M. F., Friedman, A. R., & Ruedy, R. Sulphate aerosol control of tropical Atlantic climate over the twentieth century. *Journal of Climate* 24, 2540—2555, https://doi.org/10.1175/2010jcli4065.1 (2011).

Chung, E.-S., & Soden, B. J. Hemispheric climate shifts driven by anthropogenic aerosol–cloud interactions. *Nature Geoscience* 10, 566—571, https://doi.org/10.1038/ngeo2988 (2017).

Cowan, T., & Cai, W. The impact of Asian and non-Asian anthropogenic aerosols on 20th century Asian summer monsoon.
10 *Geophysical Research Letters* 38, L11703, https://doi.org/10.1029/2011gl047268 (2011).

Dong, B., Sutton, R. T., Highwood, E. J., & Wilcox, L. J. Preferred response of the East Asian summer monsoon to local and non-local anthropogenic sulphur dioxide emissions. *Climate Dynamics* 46, 1733—1751, https://doi.org/10.1007/s00382-015-2671-5 (2016).

Dittus, A. J., Hawkins, E., Wilcox, L. J., Sutton, R. T., Smith, C. J., Andrews, M. B., & Forster, P. M. Sensitivity of historic
15 climate simulations to uncertain aerosol forcing. *Geophysical Research Letters*: in press (2020).

Fasullo, J. A mechanism for land–ocean contrasts in global monsoon trends in a warming climate. *Climate Dynamics* 39, 1137—1147, https://doi.org/10.1007/s00382-011-1270-3 (2012).

Friedman, A. R., Hwang, Y. T., Chiang, J. C. H., & Frierson, D. M. W. Interhemispheric temperature asymmetry over the twentieth century and in future projections. *Journal of Climate* 26, 5419—5433, https://doi.org/10.1175/jcli-d-12-
20 00525.1 (2013).

Guo, L, Turner, A. G., & Highwood, E. J. Impacts of 20th century aerosol emissions on the South Asian monsoon in the CMIP5 models. *Atmospheric Chemistry and Physics* 15, 6367—6378, https://doi.org/10.5194/acp-15-6367-2015 (2015).

Guo, L, Turner, A. G., & Highwood, E. J. Local and remote impacts of aerosol species on Indian summer monsoon rainfall in a GCM. *Journal of Climate* 29, 6937—6955, https://doi.org/10.1175/jcli-d-15-0728.1 (2016).

25 Hardiman, S. C., Andrews, M. B., Andrews, T., Bushell, A. C., Dunstone, N. J., Dyson, H., et al. The impact of prescribed ozone in climate projections run with HadGEM3-GC3.1. *Journal of Advances in Modelling Earth Systems* 11, https://doi.org/10.1029/2019MS001714 (2019).

Haywood, J. M., Jones, A., Dunstone, N., Milton, S., Vellinga, M., Bodas-Salcedo, A., et al. The impact of equilibriating hemispheric albedos on tropical performance in the HadGEM2-ES coupled climate model. *Geophysical Research Letters*
30 43, 395—403, https://doi.org/10.1002/2015gl066903 (2016).

Hoesly, R. M., Smith, S. J., Feng, L, Klimont, Z., Janssens-Maenhout, G., Pitkanen, T., et al. Historical (1750–2014) anthropogenic emissions of reactive gases and aerosols from the Community Emissions Data System (CEDS). *Geoscientific Model Development* 11, 369—408, https://doi.org/10.5194/gmd-11-369-2018 (2018).

Hsu, P. C., Li, T., Luo, J. J., Murakami, H., Kitoh, A., & Zhao, M. Increase of global monsoon area and precipitation under global warming: a robust signal? *Geophysical Research Letters* 39, L06701, https://doi.org/10.1029/2012gl051037 (2012).

Hsu, P. C., Li, T., Murakami, H., & Kitoh, A. Future change of the global monsoon revealed from 19 CMIP5 models. *Journal of Geophysical Research: Atmospheres* 118, 1237—1260, https://doi.org/10.1002/jgrd.50145 (2013).

5 Hsu, P. C., Li, T., & Wang, B. Trends in global monsoon area and precipitation over the past 30 years. *Geophysical Research Letters* 38, L08701, https://doi.org/10.1029/2011gl046893 (2011).

Hwang, Y. T., Frierson, D. M. W., & Kang, S. M. Anthropogenic sulphate aerosol and the southward shift of tropical precipitation in the late 20th century. *Geophysical Research Letters* 40, 2845—2850, https://doi.org/10.1002/grl.50502 (2013).

10 Jones, G. S., Stott, P. A., & Christidis, N. Attribution of observed historical near-surface temperature variations to anthropogenic and natural causes using CMIP5 simulations. *Journal of Geophysical Research: Atmospheres* 118, 4001—4024, https://doi.org/10.1002/jgrd.50239 (2013).

Kang, S. M., Seager, R., Frierson, D. M. W., & Liu, X. Croll revisited: why is the northern hemisphere warmer than the southern hemisphere? *Climate Dynamics* 44, 1457—1472, https://doi.org/10.1007/s00382-014-2147-z (2015).

15 Kuhlbrodt, T., Jones, C. G., Sellar, A., Storkey, D., Blockley, E., Stringer, M., et al. The low-resolution version of HadGEM3 GC3.1: development and evaluation for global climate. *Journal of Advances in Modelling Earth Systems* 10, 2865—2888, https://doi.org/10.1029/2018ms001370 (2018).

Kummerow, C., Simpson, J., Thiele, O., Barnes, W., Chang, A. T. C., Stocker, E., et al. The status of the Tropical Rainfall Measuring Mission (TRMM) after two years in orbit. *Journal of Applied Meteorology* 39, 1965—1982, 20 https://doi.org/10.1175/1520-0450(2001)040<1965:TSOTTR>2.0.CO;2 (2000).

Lau, K. M., & Kim, K. M. Observational relationships between aerosol and Asian monsoon rainfall, and circulation. *Geophysical Research Letters* 33, L21810, https://doi.org/10.1029/2006GL027546 (2006).

Lau, W. K. M., & Kim, K. M. Competing influences of greenhouse warming and aerosols on Asian summer monsoon circulation and rainfall. *Asia-Pacific Journal of Atmospheric Sciences* 53, 181—194, https://doi.org/10.1007/s13143-017-25 0033-4 (2017).

Levy II, H., Horowitz, L. W., Schwarzkopf, M. D., Ming, Y., Gloaz, J.-C., Naik, V., & Ramaswamy, V. The roles of aerosol direct and indirect effects in past and future climate change. *Journal of Geophysical Research: Atmospheres* 118, 4521—4532, https://doi.org/10.1002/jgrd.50192 (2013).

Li, X., Ting, M., Li, C., and Henderson, N. Mechanisms of Asian summer monsoon changes in response to anthropogenic 30 forcing in CMIP5 models. *Journal of Climate* 28, 4107—4125, https://doi.org/10.1175/JCLI-D-14-00559.1 (2015).

Liu, J., Wang, B., Ding, Q., Kuang, X., Soon, W., & Zorita, E. Centennial variations of the global monsoon precipitation in the last millennium: results from ECHO-G model. *Journal of Climate* 22, 2356—2371, https://doi.org/10.1175/2008jcli2353.1 (2009).

Morice, C. P., Kennedy, J. J., Rayner, N. A., & Jones, P. D. Quantifying uncertainties in global and regional temperature change using an ensemble of observational estimates: the HadCRUT4 dataset. *Journal of Geophysical Research* 117, D08101, https://doi.org/10.1029/2011JD017187 (2012).

Mulcahy, J. P., Jones, C., Sellar, A., Johnson, B., Boutle, I. A., Jones, A., et al. Improved aerosol processes and effective radiative forcing in HadGEM3 and UKESM1. *Journal of Advances in Modelling Earth Systems* 10, 2786—2805, https://doi.org/10.1029/2018MS001464 (2018).

Myhre, G., Shindell, D., Bréon, F. M., Collins, W., Fuglestvedt, J., Huang, J., et al. *Anthropogenic and Natural Radiative Forcing* – in *Climate Change 2013: the Physical Science Basis*. Contribution of Working Group I to the Fifth Assessment Report of the Intergovernmental Panel on Climate Change. Cambridge University Press, https://doi.org/10.1017/CBO9781107415324 (2013).

Polson, D., Bollasina, M., Hegerl, G. C., & Wilcox, L. J. Decreased monsoon precipitation in the northern hemisphere due to anthropogenic aerosols. *Geophysical Research Letters* 41, 6023—6029, https://doi.org/10.1002/2014gl060811 (2014).

Ramanathan, V., Chung, C., Kim, D., Bettge, T., Buja, L., Kiehl, J. T., et al. Atmospheric brown clouds: impacts on South Asian climate and hydrological cycle. *Proceedings of the National Academy of Sciences* 102, 5326—5333, https://doi.org/10.1073/pnas.0500656102 (2005).

Ramanathan, V., & Feng, Y. Air pollution, greenhouse gases and climate change: global and regional perspectives. *Atmospheric Environment* 43, 37—50, https://doi.org/10.1016/j.atmosenv.2008.09.063 (2009).

Rotstayn, L. D., Collier, M. A., Chrastansky, A., Jeffrey, S. J., & Luo, J.-J. Projected effects of declining aerosols in RCP4.5: unmasking global warming? *Atmospheric Chemistry and Physics* 13, 10883—10905. https://doi.org/ 10.5194/acp-13-10883-2013 (2013).

Salzmann, M., Weser, H., & Cherian, R. Robust response of Asian summer monsoon to anthropogenic aerosols in CMIP5 models. *Journal of Geophysical Research: Atmospheres* 119, 11321—11337, https://doi.org/10.1002/2014jd021783 (2014).

Samset, B. H., Lund, M. T., Bollasina, M., Myhre, G., & Wilcox, L. J. Emerging Asian aerosol patterns. *Nature Geoscience* 12, 582—586, https://doi.org/10.1038/s41561-019-0424-5 (2019).

Shonk, J. K. P., Guilyardi, E., Toniazzo, T., Woolnough, S. J., & Stockdale, T. Identifying causes of western Pacific ITCZ drift in ECMWF System 4 hindcasts. *Climate Dynamics* 50, 939—954, https://doi.org/10.1007/s00382-017-3650-9 (2018).

Slivinski, L. C., Compo, G. P., Whitaker, J. S., Sardeshmukh, P. D., Giese, B. S., McColl, C., et al. Towards a more reliable historical reanalysis: improvements for version 3 of the Twentieth Century Reanalysis system. *Quarterly Journal of the Royal Meteorological Society* 145, 2876—2908, https://doi.org/10.1002/qj.3598 (2019).

Song, F., Zhou, T., & Qian, Y. Responses of East Asian summer monsoon to natural and anthropogenic forcings in the 17 latest CMIP5 models. *Geophysical Research Letters* 41, 596—603, https://doi.org/10.1002/2013GL058705 (2014).

Stephens, G. L., Hakuba, M. Z., Hawcroft, M., Haywood, J. M., Behrangi, A., Kay, J. E., & Webster, P. J. The curious nature of the hemispheric symmetry of the Earth's water and energy balances. *Current Climate Change Reports* 2, 135—147, https://doi.org/10.1007/s40641-016-0043-9 (2016).

Taylor, K. E., Stouffer, R. J., & Meehl, G. A. An overview of CMIP5 and the experiment design. *Bulletin of the American*
5   *Meteorological Society* 93, 485—498, https://doi.org/10.1175/bams-d-11-00094.1 (2012).

Undorf, S., Polson, D., Bollasina, M. A., Ming, Y., Schurer, A., & Hegerl, G. C. Detectable impact of local and remote anthropogenic aerosols on the 20th century changes of West African and South Asian monsoon precipitation. *Journal of Geophysical Research: Atmospheres* 123, 4871—4889, https://doi.org/10.1029/2017JD027711 (2018).

Voigt, A., Pincus, R., Stevens, B., Bony, S., Boucher, O., Bellouin, N., et al. Fast and slow shifts of the zonal-mean intertropical
10   convergence zone in response to an idealised anthropogenic aerosol. *Journal of Advances in Modelling Earth Systems* 9, 870—892, https://doi.org/10.1002/2016ms000902 (2017).

Wang, B., & Ding, Q. Changes in global monsoon precipitation over the past 56 years. *Geophysical Research Letters* 33, L06711, https://doi.org/10.1029/2005gl025347 (2006).

Wang, Q., Wang, Z., & Zhang, H. Impact of anthropogenic aerosols from global, East Asian, and non-East Asian sources on
15   East   Asian   summer   monsoon   system.   *Atmospheric   Research*   183,   224—236, https://doi.org/10.1016/j.atmosres.2016.08.023 (2017).

Westervelt, D. M., Horowitz, L. W., Naik, V., Golaz, J.-C., & Mauzerall, D. L. Radiative Forcing and Climate Response to Projected   21st   Century   Aerosol   Decreases.   *Atmospheric   Chemistry   and   Physics*   15,   12681—12703, https://doi.org/10.5194/acp-15-12681-2015 (2015).

20   Wilcox, L. J., Highwood, E. J., & Dunstone, N. J. The influence of anthropogenic aerosol on multi-decadal variations of historical   global   climate.   *Environmental   Research   Letters*   8,   024033,   https://doi.org/10.1088/1748-9326/8/2/024033 (2013).

Williams, K. D., Copsey, D., Blockley, E. W., Bodas-Salcedo, A., Calvert, D., Comer, R., et al. The Met Office Global Coupled Model 3.0 and 3.1 (GC3.0 and GC3.1) configurations. *Journal of Advances in Modelling Earth Systems* 10, 357—380,
25   https://doi.org/10.1002/2017MS001115 (2018).

Wu, P., Christidis, N., & Stott, P. Anthropogenic impact on Earth's hydrological cycle. *Nature Climate Change* 3, 807—810, https://doi.org/10.1038/nclimate1932 (2013).

Xie, P., & Arkin, P. A. Global precipitation: a 17-year monthly analysis based on gauge observations, satellite estimates and numerical model outputs. *Bulletin of the American Meteorological Society* 78, 2539—2558, https://doi.org/10.1175/1520-
30   0477(1997)078<2539:GPAYMA>2.0.CO;2 (1997).

Zhou, T., Zhang, L., & Li, H. Changes in global land monsoon area and total rainfall accumulation over the last half century. *Geophysical Research Letters* 35, L16707, https://doi.org/10.1029/2008gl034881 (2008).